

Control of Electron Transfer in a Conjugated Porphyrin Dimer by Selective Excitation of Planar and Perpendicular Conformers

Mikael U. Winters,^[a] Joakim Kärnbratt,^[a] Holly E. Blades,^[b] Craig J. Wilson,^[b] Michael J. Frampton,^[b] Harry L. Anderson,^{*[b]} and Bo Albinsson^{*[a]}

Abstract: A donor–acceptor system is presented in which the electron-transfer rates can be sensitively controlled by means of excitation wavelength and temperature. The electron donor is a butadiyne-linked zinc porphyrin dimer that is connected to a C₆₀ electron acceptor. The broad distribution of conformations allowed by the butadiyne linker makes it possible to selectively excite perpendicular or planar donor conformers and thereby prepare separate initial states with driving forces for electron transfer that differ by almost

0.2 eV. This, as well as significant differences in electronic coupling, leads to distinctly different rate constants for electron transfer, which in consequence can be controlled by changing excitation wavelength. By extending the system with a secondary donor (ferrocene), a second, long-range charge-sep-

arated state can be formed. This system has been used to test the influence of conformational heterogeneity on electron transfer mediated by the porphyrin dimer in the ground state. It was found that if the dimer is forced to a planar conformation by means of a bidentate ligand, the charge recombination rate increased by an order of magnitude relative to the unconstrained system. This illustrates how control of conformation of a molecular wire can affect its behaviour.

Keywords: conformation analysis • conjugated oligomers • electron transfer • molecular switch • porphyrinoids


Introduction

Control of electron transfer is a requirement for the construction of advanced molecular electronic devices, as well as for realizing efficient artificial photosynthesis as a step towards solar energy harvesting.^[1–8] In order to build functional devices at the molecular level, versatile operational structures capable of meeting the presented demands must be synthesized, and moreover, thorough knowledge of the charge-transfer properties of these structures is required.

Donor–acceptor systems are valuable models widely used for studying photoinduced electron transfer, and are often designed for the purpose of testing the influence of specific parameters. For instance, the distance dependence of electron transfer and the influence of intervening structures have been studied extensively in geometrically well-defined donor–bridge–acceptor (D-B-A) systems.^[9–12] Today, design criteria for bridged donor–acceptor couples are well established, by a combination of experimental and theoretical work.^[13] Bridges and linkers can be chosen appropriately and the electronic coupling can thereby be sensitively tuned. The intended application determines whether the resulting systems should produce long-lived or short-lived charge-separated species.^[14–17] If the application lies in the field of solar energy, it is reasonable to aim for a system resulting in a charge-separated state for which the lifetime is long enough for further charge transfer steps to take place, thereby making it possible to move charges to an electrode interface.^[18] If, on the other hand, a structure is intended to function as a molecular wire, efficient charge transport is the goal and shallow distance dependence is therefore desirable, which in effect makes exceptionally long-lived charge-separated species less important.^[19–22]

[a] M. U. Winters, J. Kärnbratt, Prof. B. Albinsson
Department of Chemical and Biological Engineering
Physical Chemistry, Kemivägen 3, 41296 Göteborg (Sweden)
Fax: (+46) 31-772-3858
E-mail: balb@chalmers.se

[b] H. E. Blades, Dr. C. J. Wilson, Dr. M. J. Frampton,
Prof. H. L. Anderson
Department of Chemistry, University of Oxford
Chemistry Research Laboratory, Mansfield Road
Oxford OX1 3TA (UK)
Fax: (+44) 1865-275-704
E-mail: harry.anderson@chem.ox.ac.uk

 Supporting information for this article is available on the WWW under <http://www.chemeurj.org/> or from the author.

Competition between conformational dynamics and electron- and energy-transfer processes in systems containing flexible molecular bridges has been observed previously. Wasielewski and co-workers have reported on the influence of bridge dynamics in systems containing oligo-*p*-phenylene-vinyls, and found evidence for conformational gating of the donor-to-acceptor electronic coupling due to rotational dynamics.^[23] This group has moreover studied the competition between conformational relaxation and electron transfer in a series of phenothiazine-(phenyl)_{*n*}-pyrene (*n*=0, 1) donor-acceptor systems and found a strong influence on the charge-separation rate.^[24] The effect of conformation on energy transfer in directly *meso-meso* linked zinc-porphyrin arrays has been reported by Osuka, Kim, and co-workers.^[25] They concluded that conformational heterogeneity may significantly impede energy transmission through such arrays, particularly when the number of porphyrins is large. Venkataram et al. measured the conductance of seven biphenyl bridges with different ring substitutions in single-molecule junctions.^[26] The substituents served to alter the dihedral angle of the phenyl rings and it was found that the conductance was a strong function of the twist angle. Other related examples have for example been presented by Sundström and co-workers,^[27] by Guldi, Martín, Durrant and co-workers,^[28–30] as well as by Kyrchenko and Albinsson.^[31] Kinetic control by wavelength selectivity has also been reported, for example, for electron transfer processes initiated from the porphyrin S₂ state in competition with relaxation to the S₁ state.^[32–33]

In the present work, we demonstrate how the driving force for electron transfer can be tuned by selective excitation of either planar or perpendicular conformations of a conjugated porphyrin dimer (P₂), appended to a C₆₀ acceptor or bridging a ferrocene-C₆₀ donor-acceptor couple (Figure 1). The porphyrin moieties are linked by a butadiyne spacer that allows a broad distribution of conformations, and at room temperature all porphyrin-porphyrin dihedral angles are populated. Previously we have shown that the planar and perpendicular conformations of this type of porphyrin dimers are spectroscopically distinct and that it is possible to selectively excite either conformer.^[34] Further, the E₀₀ transitions of the two conformers are spaced in energy by 0.18 eV, and thus, two different initial states can be prepared that have different driving forces for electron transfer. This opens up the possibility to sensitively tune the rate for electron transfer simply by changing excitation wavelength. The formation of a long-range charge-separated state in the triad system Fc-P_{*n*}-C₆₀ (*n*=1, 2, 4) has been studied previously.^[19] When the charge-separated state Fc⁺-P_{*n*}-C₆₀⁻ is formed, the charge recombination is mediated by P_{*n*} in the ground-state, which is heterogeneous with respect to conformation. This can potentially hinder the recombination by decreasing the electronic coupling or by creating electron “traps”, particularly in longer systems. If the porphyrin dimer is forced into a planar conformation by adding the bidentate dipyrrolyl pyrrole ligand L (Figure 1), the conformational dependence of both the charge-separation and recom-

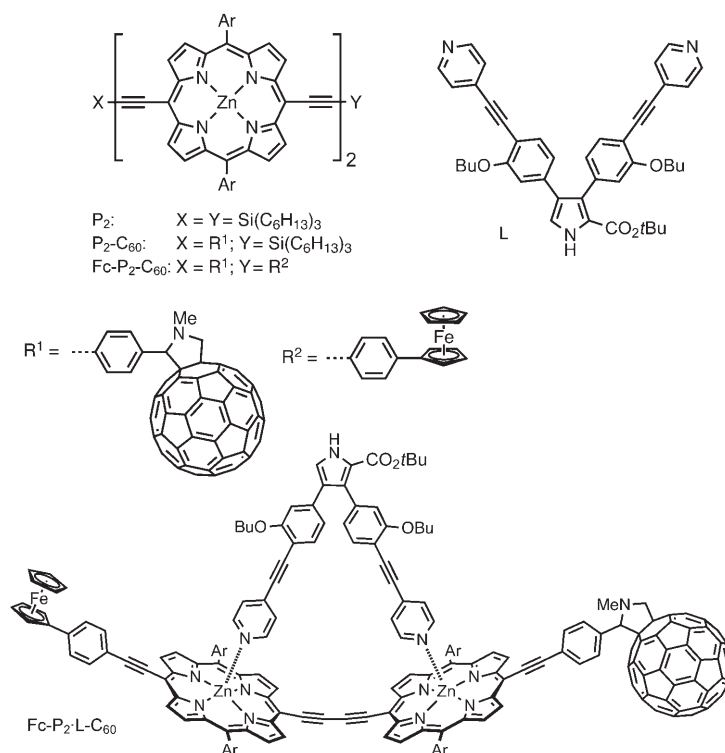


Figure 1. Porphyrin dimer (P₂) based donor-acceptor systems (P₂-C₆₀ and Fc-P₂-C₆₀) studied in this work and a dipyrrolyl pyrrole ligand (L) used to force the dimer into a planar conformation by the formation of the complex P₂/L-C₆₀. The aryl substituents, Ar, are 3,5-di(octyloxy)phenyl.

ination rate can be isolated and studied. Consequently, in this work the influence of conformation on the electron transfer properties has been studied with conformationally constrained as well as un-constrained dimers, by use of steady-state and time-resolved spectroscopy. Charge separation has been studied by using P₂-C₆₀, whereas charge recombination has been studied primarily by using Fc-P₂-C₆₀.^[19]

Results

Ground-state absorption: When the dipyrrolyl pyrrole ligand L is added to a solution of the donor-acceptor system P₂-C₆₀, a 1:1 complex (P₂/L-C₆₀) is formed in which the porphyrin macrocycles of the dimer are essentially co-planar ($K = 4 \times 10^7 \text{ M}^{-1}$ in CHCl₃).^[34] In Figure 2, the ground-state absorption spectrum of P₂-C₆₀, in CH₂Cl₂ with 0.1 vol % pyridine and in 2-methyl tetrahydrofuran (2-MTHF), as well as the spectrum of the 1:1 complex P₂-C₆₀/L in neat CH₂Cl₂, are shown. It is evident from Figure 2 that the spectral changes are dramatic when P₂-C₆₀ is forced to a planar conformation by the ligand L. The intensity of the absorption peaks at 460 and 670 nm decrease, whereas the intensity of the peaks at 495 and 735 nm increase. By analysis of fluorescence emission and excitation spectra, as well as by fluorescence lifetime studies and quantum mechanical calculations, previous

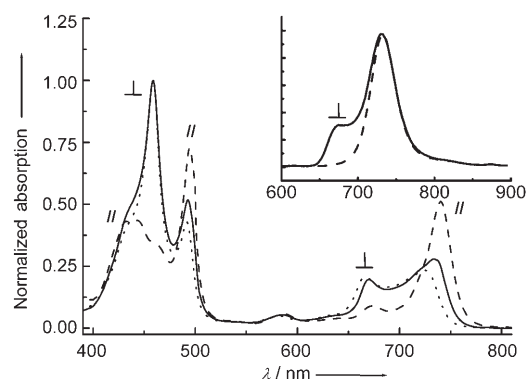
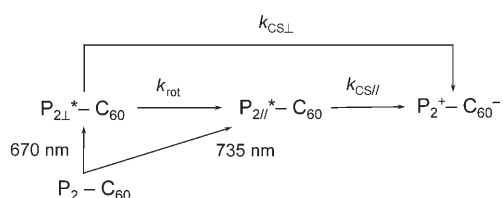


Figure 2. Absorption spectra of P_2-C_{60} in 2-MTHF (.....), in CH_2Cl_2 with 0.1 vol% pyridine (—), and in CH_2Cl_2 with the dipyrrolic pyrrole ligand L (----). The spectra of P_2-C_{60} and $P_2/L-C_{60}$ in CH_2Cl_2 are scaled by their molar absorptivity, whereas the spectrum of P_2-C_{60} in 2-MTHF is normalized to that in CH_2Cl_2 . The inset shows the emission spectra of P_2-C_{60} in 2-MTHF obtained when exciting at 460 nm (—) or at 495 nm (----). The concentration of P_2-C_{60} and L is approximately 1 μM and 2 μM , respectively.

work has assigned the peaks of the absorption spectrum of P_2 such that the high energy peaks belong to the perpendicular conformation, whereas the low energy peaks belong to the planar conformation. The barrier to rotation around the butadiyne axis is low and there is a broad continuous distribution of conformations at ambient temperature. However, the variation of the energy and intensity of the transition moments with dihedral angle results in spectral features mainly associated with the limiting cases, that is, with the planar or perpendicular conformer.^[34] Thus, the dimer can be addressed like a two-state system, and the planar and perpendicular conformer can be selectively excited by an appropriately chosen excitation wavelength (Scheme 1).



Scheme 1. Charge-separation processes and planarization of the perpendicular conformer.

Steady-state fluorescence: The fluorescence of P_2-C_{60} and $P_2/L-C_{60}$ are significantly quenched relative to P_2 , which previous work has shown is due to electron transfer. In this text it will be shown that the electron-transfer kinetics of P_2-C_{60} and $P_2/L-C_{60}$ are different due to different electronic couplings and driving forces for electron transfer. The inset in Figure 2 shows two different fluorescence spectra obtained by exciting P_2-C_{60} at 460 and 495 nm, respectively. Selectively exciting the planar population (495 or 735 nm) yields the fluorescence spectrum shown by the dashed line in Figure 2, whereas exciting the perpendicular population (460 or

670 nm) yields the spectrum shown by the solid line. The two species have unique fluorescence spectra with emission maxima at 740 (planar conformer) and 675 nm (perpendicular conformer). In the first excited singlet state, there is a considerable energy difference between the two species and the planar conformation is strongly preferred. Thus, when the perpendicular population is excited, it will relax to more planar conformations. As the two excited conformers stand in a mother–daughter relationship to each other, a portion of the initially perpendicular excited population emits at longer wavelengths, as it relaxes to a planar form at the rate $k_{rot} = 8.8 \times 10^9 \text{ s}^{-1}$ in 2-MTHF at 295 K.^[34] This, then, explains the appearance of the steady-state fluorescence spectrum obtained when exciting at 460 nm: Fluorescence from the perpendicular conformation takes place in competition with rotation around the butadiyne axis. The implication of the above, however, is that it is possible, by changing the excitation wavelength, to prepare different initial states from which an electron-transfer reaction can take place. The energy of the 0–0 transition for the two conformers differ by almost 0.2 eV, which further implies different driving forces for electron transfer (ΔG°) from the two states. By combining spectral information, which gives the 0–0 transition energies for the two conformers, $E_{00\perp}$ and $E_{00\parallel}$, with measured redox potentials, it is possible to estimate the separate driving forces (see below).

The fluorescence spectra of P_2 and P_2-C_{60} are strongly temperature dependent, as demonstrated by Figure 3. In Figure 3a, the fluorescence spectrum of P_2 , following excitation of the perpendicular population, is shown at several temperatures. As the temperature decrease, the rate for rotation from the perpendicular conformation to more planar conformations becomes slower. More and more of the emission thus appear at shorter wavelengths. However, the fluorescence spectra of P_2-C_{60} seem to vary in an unexpected way (Figure 3b). Initially, the fluorescence intensity at 740 nm decreases as temperature is lowered, but when the temperature is sufficiently low, the intensity increases dramatically. On the contrary, the emission intensity near 675 nm first increases but then decreases when the temperature is low. Moreover, the wavelengths of the peak maxima shift. This somewhat counterintuitive trend in the spectra is explained by the fact that the steady-state fluorescence spectrum of excited P_2-C_{60} , initially prepared in the perpendicular conformation, is the result of combined effects of quenching by electron transfer and planarization. The rate for rotation is more strongly temperature dependent than the rate for electron transfer from the perpendicular species. As the rotation slows down, there is a larger steady-state population of perpendicular conformers at lower temperatures, which is efficiently quenched by electron transfer and thus the emission decreases. The increase in emission at longer wavelengths is due to less efficient electron transfer from the planar species at lower temperatures. The up–down behaviour can be qualitatively reproduced by simulations using a kinetic model for the charge-transfer processes. Further, at temperatures closer to the glass temperature, the

fluorescence intensity increase at the main emission peak (740 nm) is even higher. This indicates the possibility that the quenching efficiency for a fully planar species may in fact be very low at these temperatures, and that temperature can be used to turn the electron transfer from the planar conformer off, while electron transfer from the perpendicular conformer is still efficient.

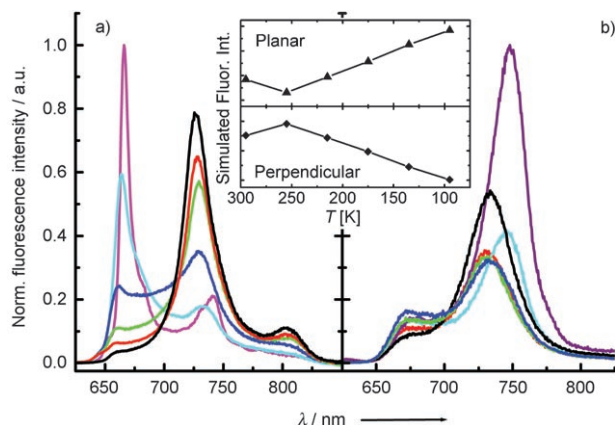


Figure 3. Emission spectra recorded at several temperatures obtained by exciting a) P_2 (2-MTHF) and b) P_2-C_{60} (2-MTHF) at 460 nm. The spectra were measured at 295 K (black), 255 K (red), 215 K (green), 175 K (blue), 135 K (cyan), 115 K (purple, P_2-C_{60} only), and 95 K (magenta, P_2 only). The inset shows the temperature variation of the integrated concentration of the planar and perpendicular species of P_2-C_{60} (top and bottom, respectively), estimated from the extracted rate constants (Tables 5 and S1, Supporting Information).

Time-resolved fluorescence: The fact that the two conformers stand in a mother–daughter relationship, makes steady-state fluorescence a less useful tool for quantitative analysis of the electron transfer kinetics that take place in P_2-C_{60} . However, the electron-transfer rate can be studied by examining the fluorescence quenching efficiency of P_2-C_{60} relative to P_2 , by way of fluorescence lifetime measurements, since electron transfer is the only additional deactivation pathway introduced by attaching the C_{60} electron acceptor, as shown previously.^[19] If this is the case, the charge-separation rate from the planar ($k_{CS\parallel}$) and perpendicular ($k_{CS\perp}$) conformer can be determined by Equation (1b) and (1a), respectively. In these equations, τ_f is the measured emission lifetime, τ_f^0 is the intrinsic lifetime of unquenched P_2 , and k_{rot} is the rate constant for rotational relaxation of the excited perpendicular conformation.^[34]

$$k_{CS\perp} = (\tau_{f\perp})^{-1} - (\tau_{f\perp}^0)^{-1} \quad (1a)$$

$$k_{CS\parallel} = (\tau_{f\parallel})^{-1} - (\tau_{f\parallel}^0)^{-1} \quad (1b)$$

In Table 1, the fluorescence lifetimes of P_2-C_{60} and $P_2/L-C_{60}$, measured at room temperature by time-correlated single photon counting (TCSPC), are listed. The samples were excited at 460 nm, and for P_2-C_{60} the emission was collected at 670 nm (perpendicular conformer) and 740 nm (planar con-

Table 1. Fluorescence lifetimes of P_2-C_{60} at room temperature, in CH_2Cl_2 with pyridine or L. The samples were excited at 460 nm. α is the normalized amplitude and f is the fractional intensity.

Emission wavelength [nm]	τ_f [ps]	α	$f^{[a]}$ [%]	χ^2
P_2-C_{60}		CH_2Cl_2 + pyridine		
670	<10 ^[b]	1.00	100	2.0 ^[b]
740	31	0.89 ^[c]	30	1.6
$P_2/L-C_{60}$		CH_2Cl_2		
740 ^[d]	28	0.91 ^[c]	40	1.5

[a] $f_i = (\alpha_i \tau_i) / \sum \alpha_i \tau_i$. [b] Resolving this lifetime is limited by the IRF. See Experimental Section. [c] Bi-exponential fit ($I(t) = \sum \alpha_j \exp(-t/\tau_j)$) was used as there were minute traces of free P_2 ($\phi_F = 20.6\%$) in the samples. τ_2 was locked to the fluorescence lifetime of P_2 (1.2 ns). [d] No fluorescence is detected at 670 nm for $P_2/L-C_{60}$. See Figure 1 (inset).

former), whereas for $P_2/L-C_{60}$ the emission was collected at 740 nm (planar conformation only). Pyridine was added to the sample not containing the ligand L, in order to reduce the possibility for effects exclusively due to complexation. As shown in Table 1, the fluorescence lifetime measured at the main emission of P_2-C_{60} agree with that of $P_2/L-C_{60}$, demonstrating that it is the planar conformer that emits. The fluorescence lifetime of the perpendicular conformer of P_2-C_{60} is too short at room temperature for the time resolution of the instrument, but it is less than half of the lifetime for the planar conformer. By using Equation (1), the data in Table 1 yield that $k_{CS\parallel} = 3.4 \times 10^{10} \text{ s}^{-1}$ and $k_{CS\perp} > 1 \times 10^{11} \text{ s}^{-1}$, at room temperature.

The rate for electron transfer is related to several parameters, such as the electronic coupling (V), the inner and outer reorganization energy accompanying the redistribution of charge (λ_i and λ_o), and the thermodynamic driving force for the electron-transfer process (ΔG°). Importantly, the rate for electron transfer is temperature dependent. The Marcus model is often used to describe diabatic electron transfer in the high temperature limit [Eq. (2)],^[35–37] and by measuring the rate for electron transfer as a function of temperature, the unknown parameters of this expression can be experimentally estimated. To this end, the fluorescence lifetimes of P_2-C_{60} were measured in 2-MTHF at low temperatures. The temperature range for this measurement was selected so that the short fluorescence lifetime of the perpendicular conformer could be properly resolved and therefore 2-MTHF was a suitable solvent. Moreover, the temperature was kept well above the glass temperature of the solvent ($T_g \approx 90 \text{ K}$). Table 2 summarizes the lifetimes obtained by fitting the fluorescence decay traces measured between 180 and 100 K. The data fits were checked by support plane analysis,^[38] which confirmed that the least-squares minimizations had converged to global minima despite the relatively high χ^2 values (See Experimental Section). In Figure 4, the logarithms of the electron-transfer rates $k_{CS\parallel}$ and $k_{CS\perp}$, multiplied by \sqrt{T} [see Eq. (2)], are plotted against the inverse temperature. By linear regression of these data, the electronic coupling and reorganization energy could be extracted (Table 3), assuming they were approximately constant in the temperature range used.

Table 2. Fluorescence lifetimes of P₂-C₆₀ in 2-MTHF measured at 670 nm ($\tau_{f\perp}$) and 740 nm ($\tau_{f\parallel}$). The samples were excited at 460 nm.

$T^{[a]}$ [K]	$\tau_{f\perp}$ [ps]	$\chi^2^{[a]}$	$\tau_{f\parallel}$ [ps]	$\chi^2^{[a]}$
180	11	1.5	29	1.7
160	12	3.0	32	1.8
140	15	2.4	37	1.4
130	16	1.3	42	1.1
120	20	1.6	44	2.1
110	22.5	2.4	54	2.6
100	27	2.4	— ^[b]	— ^[b]

[a] The measurements in a cryostat lead to unusually high χ^2 . See Experimental Section. [b] The quality of this data point was poor and it was therefore excluded.

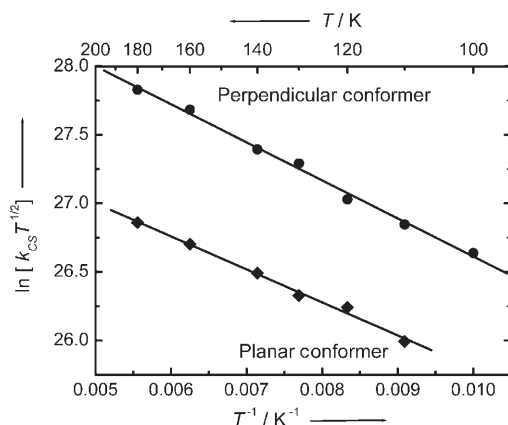


Figure 4. Rate constants for electron transfer from the perpendicular ($k_{CS\perp}$, ●) and planar ($k_{CS\parallel}$, ◆) conformer plotted against the inverse temperature. The sample was excited at 460 nm and the fluorescence lifetimes were measured at 670 and 740 nm, respectively. The lines are fits to a linear form of Equation (2).

Table 3. Driving forces for electron transfer (ΔG°), total reorganisation energies (λ_{tot}), and the electronic couplings (V) for the process P₂-C₆₀ → P₂⁺-C₆₀⁻.

Conformer	ΔG° ^[a] [eV]	λ_{tot} ^[b] [eV]	$ V $ ^[b] [cm ⁻¹]
perpendicular	-0.54	0.78	32
planar	-0.36	0.54	16

[a] Calculated from redox potentials (assuming that the oxidation potential of the perpendicular species is similar to that of the monomer P₁) and excitation energies (Equation 3). [b] Estimated by linear regression of experimental data (see Figure 4).

$$k_{CS} = \sqrt{\frac{\pi}{\hbar^2 \lambda k_B T}} |V|^2 \exp\left[-\frac{(\Delta G^\circ + \lambda)^2}{4\lambda k_B T}\right] \quad (2)$$

$$\Delta G^\circ = -E_{00} + E(P_n/P_n^+) - E(C_{60}/C_{60}^-) - e \cdot (4\pi\epsilon_0\epsilon_s R_{DA})^{-1} \quad (3)$$

The driving forces presented in the first column of Table 3 were calculated using Equation (3),^[39,40] where the energies of the 0–0 transitions were estimated from the intersection of the absorption and emission spectra (normalized to the Q-band peak of either the perpendicular or the planar con-

former). The oxidation potentials of the perpendicular and planar conformation can not be distinguished by electrochemical measurements and must be estimated. Therefore, oxidation potentials were taken from previous cyclic and square-wave voltammetry measurements on P₁ and P₂ in THF ($\epsilon_{THF}=7.52$, $\epsilon_{2-MTHF}=6.97$).^[19] Since the difference in oxidation potential between P₁ and P₂ is only about 0.02–0.04 V, it is understood that the dominant effect on the electron transfer driving forces comes from the different 0–0 transition energies, and that the difference in oxidation potentials can be neglected. The reorganisation energies λ_{tot} , can be determined from the slopes of the lines in Figure 4 by using the estimated driving forces. As the driving forces can be assessed with reasonable accuracy, and as the slopes of the lines are similar, indicating comparable activation energies for charge separation, the parameter λ_{tot} basically balances the difference in driving force between the planar and the perpendicular species. The physical interpretation of λ_{tot} is not trivial, but as rotational relaxation occur also in P₂, it is reasonable to assume that this process is not part of the reorganization accompanying the charge separation. The total reorganisation energies found are small, which is often the case for porphyrin-fullerene couples, and they compare reasonably well to values found for similar systems.^[41,42] The inner sphere reorganisation energies for C₆₀ and single porphyrins are approximately ≈ 0.06 and ≈ 0.12 eV, respectively.^[43,44] As Table 3 demonstrates, there is a significant difference in electronic coupling V between the planar and perpendicular species and the origin of this will be discussed below.

Transient absorption: In order to further characterize the influence of conformation on the electron-transfer properties of the investigated systems, transient absorption measurements using femtosecond pump-probe experiments were performed. The transient absorption spectra in Figure 5 show that the excited state absorption of the perpendicular species is different from that of the planar species. Shortly after the excitation pulse, the excited state absorption of the perpendicular species exhibits a moderately strong peak at 650 nm (Figure 5a) which is completely absent in the spectrum of the planar species (Figure 5b). The spectrum evolves, however, and approximately 100 ps after the excitation pulse, the excited-state spectrum obtained when primarily exciting the perpendicular population is more similar to that of the planar conformer, suggesting that the remaining excited population (P₂*-C₆₀) is on average more planar. The same spectral evolution was observed when the dimer, P₂, was studied (Figure S1, Supporting Information) and it was found that the transient absorption decay at 650 nm agreed with the rate for rotation determined previously by TCSPC.^[34] A similar evolution in the transient absorption spectra have been obtained for an ethyne-linked porphyrin dimer studied by the groups of Therien and Hochstrasser.^[45] The decay of the excited state absorption occurs at the rate expected from fluorescence lifetime measurements, both for measurements on a sample initially prepared in a predomi-

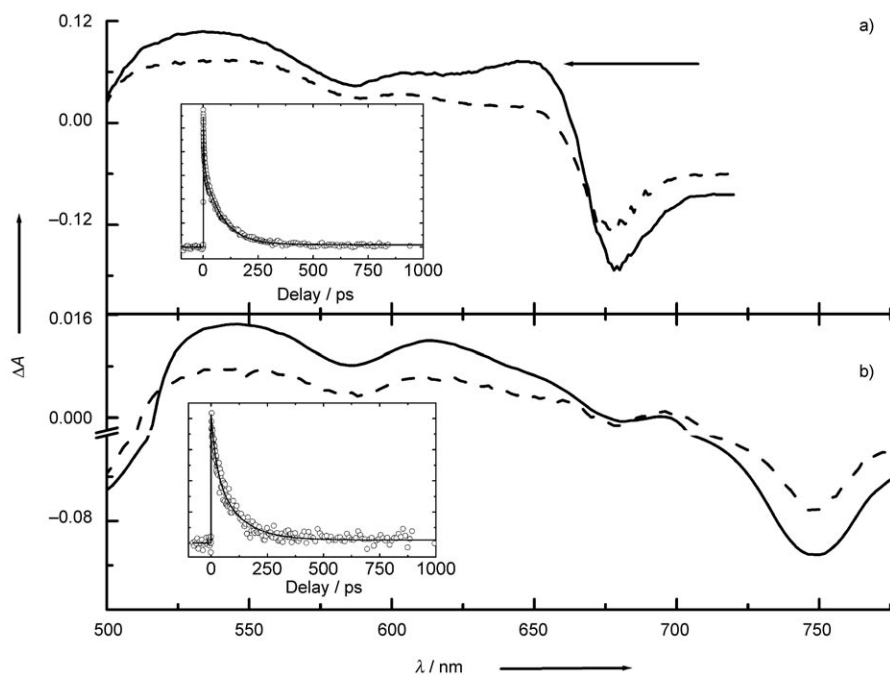


Figure 5. Transient differential absorption spectra obtained by exciting a) P_2-C_{60} (CH_2Cl_2 + 1 vol% pyridine) at 675 nm (predominantly perpendicular conformer), and b) $P_2/L-C_{60}$ in CH_2Cl_2 at 495 nm (planar conformer). The samples were probed at 1 ps (—) and 25 ps (----). The inset shows the decay of the $S_1 \rightarrow S_n$ absorption for the two samples, probed at 615 nm.

nantly perpendicular conformation and a sample containing the rotationally constrained $P_2/L-C_{60}$.

The formation of the radical species $P_2^+-C_{60}^-$ gives rise to broad unstructured absorption in the visible and intense absorption in the NIR from the porphyrin dimer radical cation. Moreover, a weaker absorption band from the fullerene radical anion is formed in the NIR. The absorption of P_2^+ ($\epsilon_{965} \approx 1.2 \times 10^5 M^{-1} cm^{-1}$) is much stronger than that of C_{60}^- ($\epsilon_{1070} \approx 1.2 \times 10^3 M^{-1} cm^{-1}$) and as the spectra partially overlap it is difficult to see a distinct peak from the fullerene anion radical in the wavelength region accessible by the experimental set-up used (450–1050 nm). However, the formation of P_2^+ is sufficient proof that the quenching of the dimer fluorescence is due to the anticipated electron-transfer process. In Figure 6a and 6b, transient absorption decay traces measured at 980 nm for P_2-C_{60} and at 1020 nm for $Fc-P_2-C_{60}$ are shown for measurements performed in CH_2Cl_2 with pyridine (Figure 6a) and in CH_2Cl_2 with the ligand L (Figure 6b). From the former system (P_2-C_{60}), the charge-separation rates for the process $P_2-C_{60} \rightarrow P_2^+-C_{60}^-$ with unconstrained (pyridine) and constrained (L) rotation were determined, and moreover, the recombination rate from $P_2^+-C_{60}^-$ for the two cases. This is a relatively uncomplicated system and this information is readily available. For the latter system ($Fc-P_2-C_{60}$), the rate for the charge shift $Fc-P_2^+-C_{60}^- \rightarrow Fc^+-P_2-C_{60}^-$ and the rate for charge recombination from the resulting fully charge-separated state $Fc^+-P_2-C_{60}^-$ could be determined with and without the ligand L. We have previously reported in detail how the fully charge-separated state $Fc^+-P_2-C_{60}^-$ is realized,^[19] but for this study we

are primarily interested in seeing how constraining the dimer to a planar conformation affects the charge recombination rate from this state, as the dimer itself is then in ground-state and therefore, in the absence of L, rotates almost freely. The ensuing conformational heterogeneity should have a dramatic effect on this rate as compared to a donor-acceptor triad in which the dimer is forced into a planar conformation. The competition between conformational dynamics and the charge recombination process is described below.

For all four systems, transient absorption data were collected at wavelengths characteristic for $S_1 \rightarrow S_n$ absorption and ground-state recovery, in addition to those characteristic for

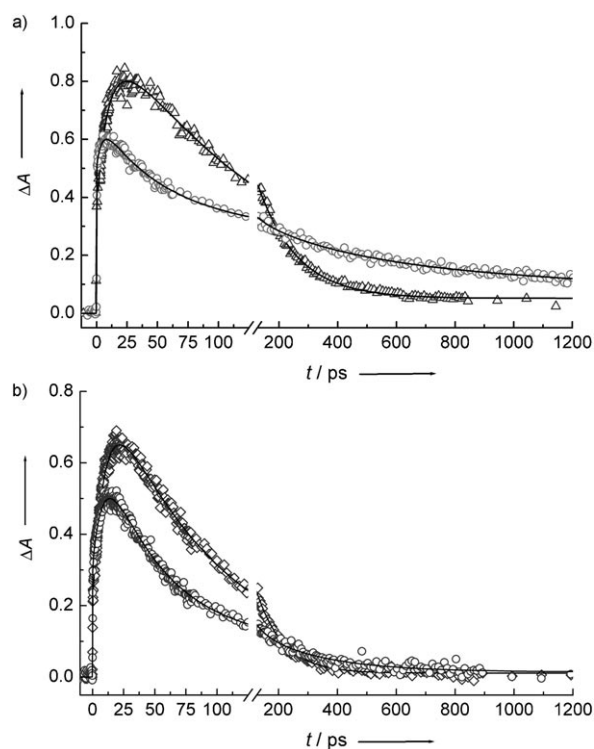


Figure 6. a) Transient absorption decays measured at 980 nm for P_2-C_{60} (triangles) and 1020 nm for $Fc-P_2-C_{60}$ (light grey circles) in CH_2Cl_2 + 1 vol% pyridine. The samples were excited at 676 nm. b) Transient absorption decays measured at 980 nm for P_2-C_{60} (diamonds) and 1020 nm for $Fc-P_2-C_{60}$ (dark grey circles) in CH_2Cl_2 + L. The samples were excited at 495 nm. In both a) and b), the differential absorption is normalized by the transient radical concentration, estimated by kinetic simulations.

radical absorption. For each individual system, the traces were fitted in a global fashion with the time constants as common parameters, using two or three exponentials with reference to the model presented in Figure 7. For P_2-C_{60} , the

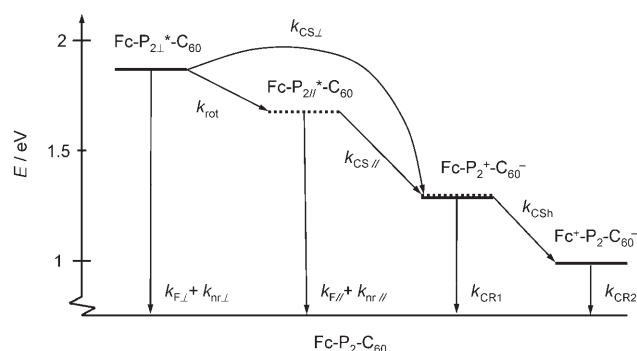


Figure 7. Relative energies of the states, electron transfer pathways and their respective rate constants.

time constants defined by Equation (4a–c) were used. Because a fraction of the planar species is initially excited in this case, a three exponential fit was necessary, whereas for $P_2/L-C_{60}$ a two exponential fit, using the time-constants defined by Equation (4b–c), was adequate. For $Fc-P_2-C_{60}$, Equation (5a–d) were used and the small fraction of initially planar species was neglected for the unconstrained system [Eq. (5a)], as the four-exponential expression resulting from including this population does not significantly benefit the analysis. In Table 4, the lifetimes that resulted from the fitting procedure are presented.

$$\tau_1 = (k_{f\perp} + k_{nr\perp} + k_{CS\perp} + k_{rot})^{-1} \quad (4a)$$

$$\tau_2 = (k_{f\parallel} + k_{nr\parallel} + k_{CS\parallel})^{-1} \quad (4b)$$

$$\tau_3 = (k_{CR1})^{-1} \quad (4c)$$

$$\tau_1 = (k_{f\perp} + k_{nr\perp} + k_{rot} + k_{CS\perp} + k_Q)^{-1} \quad (5a)$$

$$\tau_2 = (k_{f\parallel} + k_{nr\parallel} + k_{CS\parallel} + k_Q)^{-1} \quad (5b)$$

$$\tau_3 = (k_{CR1} + k_{CS,h})^{-1} \quad (5c)$$

Table 4. Lifetimes obtained by fitting transient absorption data ($S_1 \rightarrow S_n$ absorption, ground state recovery, and radical absorption) to sums of exponential decay functions.

	$\tau_1^{[a]}$ [ps]	$\tau_2^{[a]}$ [ps]	$\tau_3^{[b]}$ [ps]	$\tau_4^{[b]}$ [ps]
P_2-C_{60}	2.5	26	140	
$P_2/L-C_{60}$		12	80	
$Fc-P_2-C_{60}$	4.3 ^[c]		45	7100
$Fc-P_2/L-C_{60}$		8.8	40	700 ± 300

[a] Negative pre-exponential factor at wavelengths characteristic for radical absorption (rise). [b] Positive pre-exponential factor at wavelengths characteristic for radical absorption (decay). [c] Planarization effects are neglected.

$$\tau_4 = (k_{CR2})^{-1} \quad (5d)$$

Figure 6a shows kinetic traces for the dyad and triad systems without constrained rotation and for both there are a rise in the differential absorption due to the formation of the radical cation and anion. The rise time appears shorter for the $Fc-P_2^+-C_{60}^-$ absorption than for that of P_2-C_{60} due to a previously reported parallel energy transfer quenching process related to the ferrocene moiety,^[19] which proceeds at the rate k_Q [Eqs. (5a) and (5b)]. Further, the radical cation absorption decays faster for $Fc-P_2^+-C_{60}^-$ than for $P_2^+-C_{60}^-$ due to the charge-shift reaction forming the fully charge-shifted state ($Fc^+-P_2-C_{60}^-$). In the latter case, the transient absorption at longer delay times is exclusively from C_{60}^- . The rate constant for charge recombination from $Fc^+-P_2-C_{60}^-$ has previously been determined to approximately $1.4 \times 10^8 \text{ s}^{-1}$. The rate for the initial charge separation determined from these measurements are in agreement with fluorescence lifetime measurements as well as with the decay of the $P_2^*-C_{60}$ absorption (Table 4). The kinetic traces shown in Figure 6b represent the same measurements for rotationally constrained systems and are clearly different from those in Figure 6a. The dyad shows a simple bi-exponential kinetics as expected. For the triad, it was found that the charge shift takes place in the constrained system as well, but remarkably, the rate for charge recombination has increased dramatically to approximately $1.4 \times 10^9 \text{ s}^{-1}$. This implies that the planar conformer mediate the charge recombination in an extremely efficient manner at 25 Å donor–acceptor separation.

Discussion

In Figure 7, the relative energies of the states are shown, together with a model describing the processes taking place after photo excitation of P_2 , in either P_2-C_{60} or $Fc-P_2-C_{60}$. In the scheme, the rate constants for the processes are defined. Further, in Tables 5 and S1 (Supporting Information) values for these rate constants, extracted from the experimental data in Tables 1, 2, and 4, by reference to the presented model, are listed for each experimental technique used. Specifically, Table 5 lists the rate constants obtained from transient absorption measurements on P_2-C_{60} , which yielded the rates for the primary charge separation (k_{CS}) and the subsequent recombination (k_{CR1}), and on $Fc-P_2-C_{60}$, which further yielded the rates for the charge-shift reaction ($k_{CS,h}$, Table S1, Supporting Information) and the charge recombination of the fully charge-separated state (k_{CR2}).

The agreement between the methods used is generally good and an average value for the charge-separation rate from the perpendicular and planar conformation based on these numbers can be calculated. For charge separation from the perpendicular species, the rate is approximately $2.5 \times 10^{11} \text{ s}^{-1}$, whereas the rate for charge separation from the planar species is approximately $5.8 \times 10^{10} \text{ s}^{-1}$. That is, charge separation is roughly four times faster from the perpendicular conformation than from the planar conformation.

Table 5. First-order rate constants (k) for the excited state reactions defined in Figure 7.

	P_2-C_{60} ^[a] [s ⁻¹]	Fc- P_2 - C_{60} [s ⁻¹]	$P_2/L-C_{60}$ ^[b] [s ⁻¹]	Fc- $P_2/L-C_{60}$ ^[b] [s ⁻¹]
$k_{CS\perp}$	3.9×10^{11}	2.0×10^{11}	–	–
$k_{CS\parallel}$	3.8×10^{10}	–	8.3×10^{10}	8.3×10^{10}
k_{CR1}	7.1×10^9	–	1.3×10^{10}	–
k_{CR2}	–	1.4×10^8	–	1.4×10^9

[a] Transient adsorption data (CH₂Cl₂ + pyridine). The samples were excited at 676 nm. [b] Transient adsorption data (CH₂Cl₂ + L). The samples were excited at 495 nm.

The activation energies for charge separation (ΔG^\ddagger) of the perpendicular and planar species are both very small, and in the solvent used for these experiments they are approximately equal. This indicates that the electron transfer processes take place near the top of the so-called Marcus parabola. As demonstrated in Table 3, the higher rate for charge separation from the perpendicular conformer is mainly due to a greater electronic coupling in combination with the higher driving force for electron transfer. This analysis was done by using the classical Marcus equation. The more advanced semiclassical formulation of Jortner and co-workers gave very similar results, and the conclusion is that the most important parameter for the different electron-transfer rates is the electronic coupling.^[46,47] It is important to realize that only the limiting cases, a perpendicular and a fully planar conformation, are considered explicitly in this discussion. However, by changing the excitation wavelength, a conformer with an arbitrary porphyrin–porphyrin dihedral angle $\phi \pm \Delta\phi$ can be addressed and possibly a rate for electron transfer can thereby be chosen. Because of the continuous distribution of conformations, the selectivity will be limited to a region $\Delta\phi$ determined by the width of the absorption bands and the monochromaticity of the excitation light source. The driving force and electronic coupling will probably not change abruptly, but vary smoothly as an on average more and more planar population will be addressed when the excitation wavelength is changed from shorter to longer Q-band wavelengths. The extreme cases are uniquely selected to a high degree by choosing energies matching the far edges of the Q-band absorption.

It is interesting that charge recombination ($P_2^+-C_{60}^- \rightarrow P_2-C_{60}$) is faster for the dyad constrained to a planar conformation than it is for the unconstrained dyad. The majority of the perpendicular population should undergo charge separation ($k_{CS\perp} = 2.5 \times 10^{11} \text{ s}^{-1}$) before having a chance to rotate to a more planar conformation ($k_{rot} = 8.8 \times 10^9 \text{ s}^{-1}$). However, after the charge separation, twisting to a more planar conformation is still advantageous as it leads to an energy gain related to the delocalization of the positive charge.^[48] The perpendicular species $P_{2\perp}^+-C_{60}^-$ will thus twist to smaller dihedral angles and may undergo charge recombination anywhere between 0–90°, whereas the constrained system is always nearly planar. This implies that planarity somehow

favours the charge recombination, since this process is faster for the constrained system.

The charge-shift reaction ($Fc-P_2^+-C_{60}^- \rightarrow Fc^+-P_2-C_{60}^-$) proceeds at approximately the same rate for the constrained ($Fc-P_2/L-C_{60}$) and unconstrained systems ($Fc-P_2-C_{60}$), which means that the quantum yields for this process are 48 and 68%, respectively, mainly due to the faster recombination of $P_2^+/L-C_{60}^-$ ($\Phi_{CSH} = k_{CSH}/(k_{CR1} + k_{CSH})$). Further, the slower primary charge separation from the planar conformation, means that the overall quantum yield for the fully charge-separated state is only 35% for $Fc-P_2/L-C_{60}$, but 58% for $Fc-P_2-C_{60}$, based on transient absorption data ($\Phi = k_{CS}/(k_F + k_{nr} + k_{CS} + k_Q) \times \Phi_{CSH}$). The low quantum yield for the fully charge-separated state $Fc^+-P_2/L-C_{60}^-$, in addition to the low molar absorptivity of C_{60}^- at the probed wavelength, explains the weak transient signal detected (Figure 6b). Moreover, the recombination is faster by an order of magnitude for this system relative to the conformationally heterogeneous system ($Fc^+-P_2-C_{60}^-$). The rate for this recombination is approximately $1\text{--}2.5 \times 10^9 \text{ s}^{-1}$, but the poor signal makes it difficult to determine this rate with high accuracy. The faster recombination of the planar system can be explained by the higher degree of conjugation in the planar system. Charge is mediated more efficiently by a delocalized system, and this is shown by the larger electronic coupling obtained for the planar system if the charge-recombination process is treated with a simple Marcus approach. Using a reorganization energy typical for ferrocene–fullerene couples (1.2 eV),^[16,49] the electronic coupling for the planar system was estimated to $2.5\text{--}3.9 \text{ cm}^{-1}$, which is significantly higher than the coupling in the conformationally heterogeneous system (0.92 cm^{-1}). This result points to the importance of controlling the structure and possible conformational distributions of molecular wires.

Conclusion

Photoinduced electron transfer in a donor–acceptor dyad, P_2-C_{60} , has been studied by time-resolved and steady-state spectroscopic methods. The electron-transfer rate was significantly faster from the conformationally distorted singlet excited donor ($P_{2\perp}$) than from the planar conformer ($P_{2\parallel}$). This was expected, as more energy (approximately 0.2 eV) is “stored” in excited $P_{2\perp}$, making the driving force for electron transfer larger from the perpendicular species. However, analysis of the temperature dependence of the fluorescence quenching showed that both processes had similar activation energies (i.e., the same slopes in Figure 4), but significantly different pre-exponential factors. In terms of the Marcus theory of electron transfer this means that the different rates for electron transfer reactions from $P_{2\perp}$ and $P_{2\parallel}$ must be ascribed to the significant difference in the electronic coupling. It is interesting to consider the reasons to why the perpendicular conformer has a larger electronic coupling to the appended C_{60} than the planar conformer. In the excited state of the perpendicular conformation of the

dimer it is likely that the excitation is localized on one porphyrin unit, and that such localization quickly places the excited state on the porphyrin fragment that is closest to the C₆₀ acceptor and thereby makes the average donor–acceptor distance shorter. A similar localization is not favourable for the fully planar system where the inter-porphyrin conjugation is larger, which may explain the lower electronic coupling.

The fact that simply changing the excitation energy changes the dynamics of the system will be an important handle for directing electrons in a charge-separation reaction. This property can be optimized by the molecular components or possibly by just changing the solvent polarity. Ultimately, an “on/off” situation would be highly desirable, because this would constitute a simple charge-separation switch.

Experimental Section

Materials: The solvents used for this study was dichloromethane (CH₂Cl₂, ACROS) and 2-methyl tetrahydrofuran (2-MTHF, ACROS). The solvents were always freshly distilled when used. When dichloromethane was used, approximately 0.1 vol% pyridine was added in order to make the measurements comparable to those performed using the dipyrrolyl pyrrole ligand (Figure 1). The synthesis of these compounds have been reported previously.^[19,50]

Spectroscopy: Absorption spectra were measured on a Cary 4B UV/Vis spectrophotometer. The spectra were recorded between 300 and 850 nm at 300 nm per min with 0.5 nm spectral bandwidth. The sample was contained in a 10 mm quartz cuvette and a new baseline was recorded for each sample. Fully corrected emission spectra were recorded on a Spex Fluorolog 3 equipped with a xenon lamp. To avoid aggregation and inner-filter effects, the concentrations of the samples were low in the fluorescence measurements, approximately 0.1–4 μM in most cases. The spectral bandwidth for the emission and excitation monochromators was between 1–4 nm and was chosen in order to get a good signal-to-noise ratio. Time-resolved fluorescence measurements were done by time-correlated single photon counting (TCSPC). The excitation pulse was provided by a Tsunami Ti/sapphire laser (Spectra-Physics) which was pumped by a Millennia Pro X (Spectra-Physics). The Tsunami output was tuned to either 920 or 990 nm and subsequently frequency doubled to 460 or 495 nm. A pulse selector (Model 3980, Spectra Physics) was used to achieve a 4 MHz repetition rate, when necessary. The emission photons were collected by a thermoelectrically cooled micro-channel plate photomultiplier tube (R3809U-50, Hamamatsu), yielding a time-resolution of 10–20 ps. The signal was digitalized using a multi-channel analyzer with 4096 channels (SPC-300, Edinburgh Analytical Instruments) and in order to get a good statistics at least 10000 counts (top channel) were recorded for each decay. The fluorescence decay curves were fitted to two-exponential expressions by the program FluoFit Pro v.4 (PicoQuant GMBH), individually as well as with global parameters.

Temperature studies: For the temperature dependent absorption and emission studies, a cryostat (Oxford Instruments) cooled by liquid nitrogen was used. The samples were degassed by repeated freeze-pump-thaw cycles (final pressure < 10⁻⁴ Torr) prior to measurements to exclude any effects due to quenching reactions caused by oxygen. Using a cryostat for TCSPC measurements introduce difficulties when the fluorescence lifetimes are short, since the instrument response function contains more scattered light in this case. χ^2 thus become larger than normal. In particular, this is a problem when the emission intensity is weak.

Transient absorption: A pump-probe set up was used to record transient absorption spectra and transient absorption decays. A Ti/sapphire oscillator (Tsunami, Spectra Physics) generating pulses approximately 90 fs

broad (FWHM) was used to seed a Ti/sapphire regenerative amplifier (Spitfire, Spectra Physics) that was pumped by a frequency-doubled diode-pumped Nd:YLF laser (Evolution-X, Spectra Physics) and produced pulses approximately 110 fs long (FWHM). The amplified laser beam (790 nm) was divided by a 70:30 beam-splitter and the two beams were subsequently used as pump and probe. The pump beam was manipulated by an OPA (TOPAS, Light Conversion Ltd) to yield 495 or 660 nm and was delayed relative to the probe pulse by either one of two available optical delay lines (1.6 or 10 ns). The probe beam was obtained by focusing the remaining IR on a 1 mm sapphire plate, which generated a continuum from 450–1050 nm. The probe was subsequently divided into a reference beam and a probe beam, and the latter of these was overlapped by the pump at the sample. When spectra and decays were measured in the near-infrared, a combination of long-wave pass filters were used in order to completely block out visible light, otherwise the detected signal was dominated by secondary diffraction maxima from the monochromator used (TRIAX 180, ISA Instruments). All porphyrins have strong triplet absorption at approximately 500 nm, which without appropriate filters give strong, long-lived transient absorption signals at 1000 nm. The samples were dissolved in freshly distilled solvent deoxygenated by argon bubbling, and the optical density was approximately 1 at the excitation wavelength. The samples were contained in a moving 1 mm cuvette and excited at a 500 Hz repetition rate. The recorded traces were fitted individually and globally to a sum of exponentials convoluted with the cross-correlated pump and probe pulse (simulated by Gaussian pulse profiles) with home-made routines (MATLAB, Mathworks Inc.).

Acknowledgement

This work was funded by the Swedish Research Council (VR), the Knut and Alice Wallenberg Foundation, and EPSRC.

- [1] V. Balzani, *Photochem. Photobiol. Sci.* **2003**, *78*, 459–476.
- [2] M. A. Ratner, *Materials Today* **2002**, *5*, 20–27.
- [3] P. Ball, *Nature* **2000**, *406*, 118–120.
- [4] A. K. Burrell, M. R. Wasielewski, *J. Porphyrins Phthalocyanines* **2000**, *4*, 401–406.
- [5] J. M. Tour, *Acc. Chem. Res.* **2000**, *33*, 791–804.
- [6] H. Imahori, Y. Mori, Y. Matano, *J. Photochem. Photobiol. C* **2003**, *4*, 51–83.
- [7] D. Gust, T. A. Moore, A. L. Moore, *Acc. Chem. Res.* **2001**, *34*, 40–48.
- [8] M. R. Wasielewski, *Chem. Rev.* **1992**, *92*, 435–461.
- [9] K. Pettersson, J. Wiberg, T. Ljungdahl, J. Martensson, B. Albinsson, *J. Phys. Chem. A* **2006**, *110*, 319–326.
- [10] K. Kilsa, J. Kajanus, A. N. Macpherson, J. Martensson, B. Albinsson, *J. Am. Chem. Soc.* **2001**, *123*, 3069–3080.
- [11] H. A. Clayton, K. P. Ghiggino, J. M. Lawson, M. N. Paddon-Row, *J. Photochem. Photobiol. A* **1994**, *80*, 323–331.
- [12] A. Helms, D. Heiler, G. McLendon, *J. Am. Chem. Soc.* **1992**, *114*, 6227–6238.
- [13] B. Albinsson, J. Mårtensson, *Controlling excitation energy and electron transfer by tuning the electronic coupling*, World Scientific Publishing, Singapore, **2005**.
- [14] A. Harriman, *Angew. Chem.* **2004**, *116*, 5093–5095; *Angew. Chem. Int. Ed.* **2004**, *43*, 4985–4987.
- [15] H. Imahori, K. Tamaki, Y. Araki, T. Hasobe, O. Ito, A. Shimomura, S. Kundu, T. Okada, Y. Sakata, S. Fukuzumi, *J. Phys. Chem. A* **2002**, *106*, 2803–2814.
- [16] H. Imahori, K. Tamaki, D. M. Guldi, C. P. Luo, M. Fujitsuka, O. Ito, Y. Sakata, S. Fukuzumi, *J. Am. Chem. Soc.* **2001**, *123*, 2607–2617.
- [17] H. Imahori, K. Hagiwara, M. Aoki, T. Akiyama, S. Taniguchi, T. Okada, M. Shirakawa, Y. Sakata, *J. Am. Chem. Soc.* **1996**, *118*, 11771–11782.

- [18] H. Imahori, S. Fukuzumi, *Adv. Funct. Mater.* **2004**, *14*, 525–536.
- [19] M. U. Winters, E. Dahlstedt, H. E. Blades, C. J. Wilson, M. J. Framp-ton, H. L. Anderson, B. Albinsson, *J. Am. Chem. Soc.* **2007**, *129*, 4291–4297.
- [20] A. Harriman, S. A. Rostron, A. Khatyr, R. Ziessel, *Faraday Discuss.* **2006**, *131*, 377–391.
- [21] F. Giacalone, J. L. Segura, N. Martin, D. M. Guldi, *J. Am. Chem. Soc.* **2004**, *126*, 5340–5341.
- [22] W. B. Davis, W. A. Svec, M. A. Ratner, M. R. Wasielewski, *Nature* **1998**, *396*, 60–63.
- [23] W. B. Davis, M. A. Ratner, M. R. Wasielewski, *J. Am. Chem. Soc.* **2001**, *123*, 7877–7886.
- [24] J. Daub, R. Engl, J. Kurzawa, S. E. Miller, S. Schneider, A. Stockmann, M. R. Wasielewski, *J. Phys. Chem. A* **2001**, *105*, 5655–5665.
- [25] T. K. Ahn, Z. S. Yoon, I. W. Hwang, J. K. Lim, H. Rhee, T. Joo, E. Sim, S. K. Kim, N. Aratani, A. Osuka, D. Kim, *J. Phys. Chem. B* **2005**, *109*, 11223–11230.
- [26] L. Venkataraman, J. E. Klare, C. Nuckolls, M. S. Hybertsen, M. L. Steigerwald, *Nature* **2006**, *442*, 904–907.
- [27] M. Chachisvilis, V. S. Chirvony, A. M. Shulga, B. Kallebring, S. Larsson, V. Sundstrom, *J. Phys. Chem.* **1996**, *100*, 13867–13873.
- [28] S. Handa, F. Giacalone, S. A. Haque, E. Palomares, N. Martín, J. R. Durrant, *Chem. Eur. J.* **2005**, *11*, 7440–7447.
- [29] D. M. Guldi, F. Giacalone, G. de la Torre, J. L. Segura, N. Martín, *Chem. Eur. J.* **2005**, *11*, 7199–7210.
- [30] G. de la Torre, F. Giacalone, J. L. Segura, N. Martín, D. M. Guldi, *Chem. Eur. J.* **2005**, *11*, 1267–1280.
- [31] A. Kyrchenko, B. Albinsson, *Chem. Phys. Lett.* **2002**, *366*, 291–299.
- [32] D. Le Gourrierec, M. Andersson, J. Davidsson, E. Mukhtar, L. C. Sun, L. Hammarström, *J. Phys. Chem. A* **1999**, *103*, 557–559; R. T. Hayes, C. J. Walsh, M. R. Wasielewski, *J. Phys. Chem. A* **2004**, *108*, 2375–2381.
- [33] A. C. Benniston, G. M. Chapman, A. Harriman, M. Mehrabi, *J. Phys. Chem. A* **2004**, *108*, 9026–9039.
- [34] M. U. Winters, J. Kärnbratt, C. J. Wilson, H. L. Anderson, B. Albinsson, *J. Phys. Chem. C* **2007**, *111*, 7192–7199.
- [35] R. A. Marcus, *J. Chem. Phys.* **1956**, *24*, 966–978.
- [36] R. A. Marcus, *Can. J. Chem.* **1959**, *37*, 155–163.
- [37] R. A. Marcus, N. Sutin, *Biochim. Biophys. Acta* **1985**, *811*, 265–322.
- [38] M. Straume, S. G. Frasier-Cadoret, M. L. Johnson, *Least-squares Analysis of Fluorescence Data*, Plenum Press, New York, **1991**, p. 177–239.
- [39] D. Rehm, A. Weller, *Ber. Bunsen-Ges. Phys. Chem.* **1969**, *73*, 834–839.
- [40] A. Weller, *Z. Phys. Chem. (Muenchen Ger.)* **1982**, *133*, 93–98.
- [41] H. Imahori, H. Yamada, D. M. Guldi, Y. Endo, A. Shimomura, S. Kundu, K. Yamada, T. Okada, Y. Sakata, S. Fukuzumi, *Angew. Chem.* **2002**, *114*, 2450–2453; *Angew. Chem. Int. Ed.* **2002**, *41*, 2344–2347.
- [42] D. M. Guldi, *Chem. Soc. Rev.* **2002**, *31*, 22–36.
- [43] S. Larsson, A. Klimkans, L. Rodriguez-Monge, G. Duskesas, *THEO-CHEM* **1998**, *425*, 155–159.
- [44] X. Amashukeli, N. E. Gruhn, D. L. Lichtenberger, J. R. Winkler, H. B. Gray, *J. Am. Chem. Soc.* **2004**, *126*, 15566–15571.
- [45] R. Kumble, S. Palese, V. S. Y. Lin, M. J. Therien, R. M. Hochstrasser, *J. Am. Chem. Soc.* **1998**, *120*, 11489–11498.
- [46] J. Ulstrup, J. Jortner, *J. Chem. Phys.* **1975**, *63*, 4358–4368.
- [47] J. Jortner, M. Bixon, *J. Chem. Phys.* **1988**, *88*, 167–170.
- [48] H. L. Anderson, *Chem. Commun.* **1999**, 2323–2330.
- [49] D. M. Guldi, H. Imahori, K. Tamaki, Y. Kashiwagi, H. Yamada, Y. Sakata, S. Fukuzumi, *J. Phys. Chem. A* **2004**, *108*, 541–548.
- [50] M. Hoffmann, C. J. Wilson, B. Odell, H. L. Anderson, *Angew. Chem.* **2007**, *119*, 3183–3186; *Angew. Chem. Int. Ed.* **2007**, *46*, 3122–3125.

Received: March 20, 2007

Published online: June 21, 2007